https://doi.org/10.5194/egusphere-2024-852
Preprint. Discussion started: 28 March 2024

The influence of vertical lithological contrasts on strike-slip fault behavior: Insights from analogue models.

Sandra González-Muñoz[1], Guido Schreurs[2], Timothy Schmid[2], Fidel Martín-González[1]

[1]Área de Geología - ESCET, TECVOLRISK Research Group, Universidad Rey Juan Carlos. C/Tulipan s/n, Mostoles, 28933 Madrid, Spain
[2] Institute of Geological Sciences, University of Bern, Bern, Switzerland

Correspondence to: Sandra González Muñoz (sandra.gonzalezmu@urjc.es)

Abstract

This work investigates the influence of rheological contrasts on the nucleation and behavior of strike-slip faults. To achieve this, we have carried out a series of brittle-viscous strike-slip shear analogue models, using quartz sand and microbeads as granular materials with different internal friction and cohesion values. Particle Imaging Velocimetry (PIV) was applied to time-series of surface images to calculate incremental and cumulative strains. Understanding how strike-slip faults nucleate and interact in the heterogeneous upper crust is relevant in seismic hazard analysis and geothermal and hydrocarbon exploration. To reproduce the heterogeneity of the upper crust, three sets of experiments we performed: 1) upper layer composed either of quartz sand or microbeads; 2) upper layer with a vertical contrast i.e., quartz sand surrounded by microbeads and vice-versa; and 3) same set-up as in the previous set but changing the orientation of the vertical contrast. Our study shows that the introduction of an upper crustal vertical contrast influences the behavior and evolution of strike-slip faults. The models containing a vertical contrast were more complex and induced a compartmentalization of the model. The initial fault strike is related to the material's properties. However, this initial strike changes when faults crosscut the materials with less internal friction angle clockwise, and anticlockwise when the contrast has higher internal friction angle. Areas containing materials with less internal friction angle take longer to localized the deformation, but they show a greater number of faults. The biggest increase in the number of synthetic and antithetic faults occurs with the introduction of vertical contrast. These results were compared with the intraplate fault systems of the NW Iberian Peninsula, focusing on the Penacova-Régua-Verin and Manteigas-Vilariça-

Bragança fault systems. They are major left-lateral faults that cross-cut lithologies characterized by vertical rheological contrasts, with deformation patterns similar to those observed in our analogue models.

Keywords

Strike-slip fault zone, Fault segmentation, Rheological contrasts, Analogue modelling

1. Introduction

The structural styles and the factors that control the geometry of strike-slip faults have been investigated in detail in many studies (e.g. Riedel, 1929; Anderson, 1951; Deng et al., 1986; Sylvester, 1988; Dooley and Schreurs, 2012; Lefevre et al., 2020a). In nature, strike-slip fault systems typically have complex architectures consisting of numerous segments separated by steps or of anastomosing, linked fault zones (Aydin and Nur, 1982; Barka and Kadinsky-Cade, 1988; Wesnousky, 1988; Stirling et al., 1996; Kim et al., 2004). How faults interact or link is considered to be a function of loading, stress disturbances, rheology and the geometry of pre-existing structures (Kim et al., 2004; Myers and Aydin, 2004; Peacock and Sanderson, 1991, 1992; Burgmann and Pollard, 1994; Sibson, 1985; Gamond, 1983; Rispoli, 1981; Wesnousky, 1988).

Understanding fault interaction and linkage is important not only in view of the location of geothermal and hydrocarbon resources (Sibson, 1985; Martel and Peterson, 1991; Aydin, 2000; Odling et al., 2004; Cazarin et al., 2021) but also for its implications on regional stress orientations (Kirkland et al., 2008), as well as seismic hazard (Petersen et al., 2011), in terms of dynamics, fault growth and size of earthquakes (Aki, 1989; Harris and Day, 1999; Scholz, 2002; Wesnousky, 2006; Shaw and Dieterich, 2007; de Joussineau and Aydin, 2009; Preuss et al., 2019).

Various studies have investigated the influence of horizontal rheological contrasts (e.g., mechanical stratigraphy of sedimentary sequences) on fault orientation, segmentation, linkage, and displacement, using field observations (e.g., Peacock and Sanderson, 1992), combining with analytical and numerical methods (Du and Aydin, 1995; Aydin and Berryman, 2010; De Dontney et al., 2011), and analogue models (Richard, 1991; Richard et al., 1995; Gomes et al., 2019; Venancio and Alves Da Silva, 2023). However, only the

https://doi.org/10.5194/egusphere-2024-852
Preprint. Discussion started: 28 March 2024

study from Gomes et al (2019) has investigated systematically the influence of vertical rheological contrast in strike-slip fault behavior, using silicone as weak body immersed in between the horizontal layers of the model. The strike-slip fault behaviour trough changes in the rheological properties of the upper crust is of particular importance in the context of strike-slip fault zones. As a consequence of their long aspect ratio (i.e. ratio length vs width), they often cut across pre-existing tectonic contacts with steeply oriented and contrasting rheologies.

In this study, we use scaled analogue model experiments to assess the role of vertical rheological contrasts in the upper crust on fault kinematics in distributed strike-slip shear. The results obtained show how the vertical contrast influences the orientation, evolution and number of faults. The obtained results are compared with one natural example in the NW part of the Iberian Peninsula, where two large parallel strike-slip sinistral fault systems cut lithologies with contrasting brittle rheologies.

2. Methods

2.1. Analogue model setup and monitoring

In this study, eight simple shear experiments are presented. The experimental machine comprises a mobile base plate that can be translated horizontally along a fixed base plate (Fig. 1). An assemblage of 60 plexiglass bars (each 79 cm long, 5 cm high and 5 mm wide) overlies the two base plates, which are confined by two longitudinal carbon-fiber sidewalls (Fig. 1b) and two short sidewalls consisting of vertical rubber sheets. The analogue model is constructed on top of the plexiglass bars and consists of a 2 cm-thick viscous layer and a 2 cm-thick brittle layer, to simulate the lower and upper crust respectively. In this way, we avoid the possible boundary effects due to the interaction between the brittle materials and the plexiglass bars. Initially, the horizontal model dimensions in each model are 78 cm x 30 cm. The movement of the mobile plate occurred by computer-controlled stepper motors providing a constant velocity of 40 mm/h in all experiments, obtaining 80 mm of total displacement after two hours. The displacement of the basal mobile plate results in a distributed sinistral strike-slip shear movement in the overlying model materials. The systematics followed throughout this work includes four series of experiments (Fig. 2; Series A, B, C and D). Series A involved two reference models with only one brittle material (Fig. 3a), either quartz sand or microbeads (MB), to investigate fault kinematics in models without any vertical rheological contrast. The following three series simulated vertical rheological contrasts by adding a c. 5 cm wide central band

https://doi.org/10.5194/egusphere-2024-852
Preprint. Discussion started: 28 March 2024

composed of quartz sand with microbeads on either side or vice versa (Fig. 2; Series B, C, and D). Two vertical thin sheets of cardboard (< 1 mm) were first placed as provisional walls, spaced 5 cm apart, on top of the viscous layer in the central domain of the model. Subsequently, the different granular materials were sieved on top and once the desired model thickness was reached, the cardboard sheets were carefully removed. Hence, we obtained two vertical rheological contrasts that consist of reactivated lithological boundaries. For descriptive purposes, we assign a N orientation parallel to the short sides of the undeformed model. Considering this, three different vertical contrast orientations were tested: N-S (Series B), N20°W (Series C), and N20°E (Series D). With the addition of the central contrast, we distinguish three domains in our model descriptions: a western domain, a central domain (i.e., the band of contrasting material), and an eastern domain.

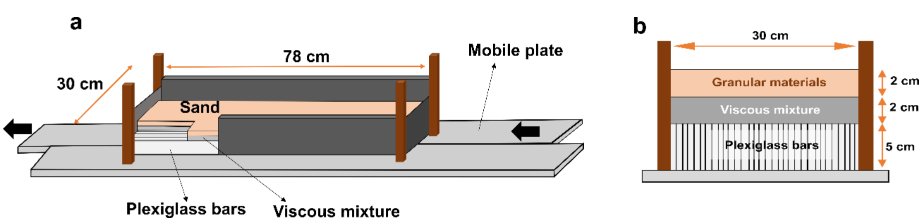

Figure 1: Experimental setup for conducted experiments. A) Schematic representation of the sandbox. The base of the model set-up consists of a fixed plate and a mobile wall. The model is confined by two short sidewalls, consisting of rubber sheets and two long sidewalls. B) Model setup cross sections, showing the assemblage of plexiglass bars below the model materials.

The different experiments were monitored by an automated Nikon D810 (36 MPx) DSLR camera positioned above the experimental model. Images were taken at intervals of 30 sec during two hours, resulting in 240 pictures in total. For a quantitative 2D analysis of the surface deformation, we used the StrainMaster module of the LaVision© DaVis image correlation software. This software allows us to do the camera calibration, the mapping function for image correlation, and the displacement calculation by using a square matching algorithm with adaptive multi-pass cross-correlation. We use subsets of 31 by 31 pixels with a 75% overlap for the displacement calculations. The pictures obtained have an average area of 8256 by 5504 pixels for the X and Y axis, respectively, with an average resolution of 300 pixels.

https://doi.org/10.5194/egusphere-2024-852
Preprint. Discussion started: 28 March 2024

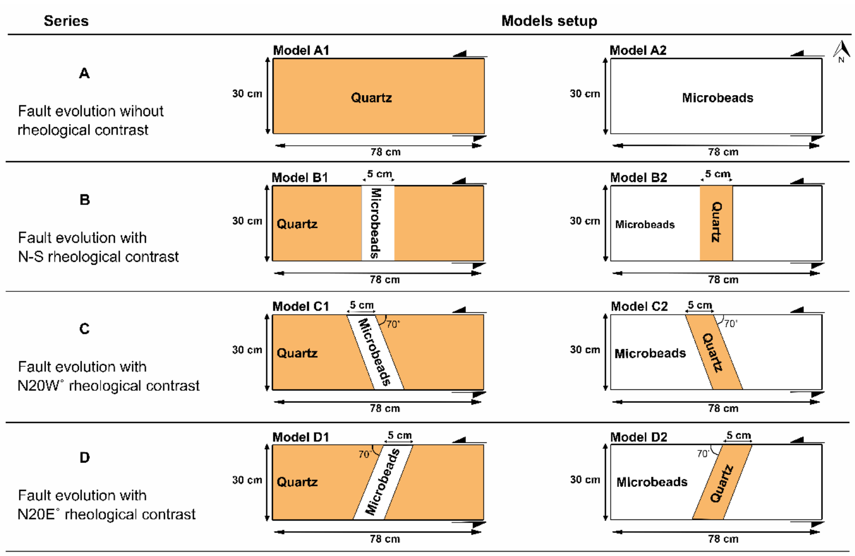

Figure 2: Schematic top views of the four series of models, with dimensions and materials used in each series.

Since the experiments were conducted using a simple shear setup (see Fig. 1a), vertical motions during deformation were negligible, with all the movement located within the horizontal plane. The quantitative deformation analysis included: (1) scaling and rectifying top view images; (2) subsequent displacement calculation and; (3) the application of statistical analysis representing the dominant fault orientations, measured every 2 cm, in rose diagrams. The DaVis software calculates incremental displacement fields based on a direct correlation algorithm and provides access to individual displacement components. We used the z-vorticity ω_z (i.e., a local measure of rotation within the xy-plane) as a proxy for shear movement along strike-slip faults. In contrast to the shear strain ε_{xy}, vorticity is not dependent on the orientation of the coordinate system, which is crucial when quantifying deformation along faults that strike obliquely with respect to the coordinate system (e.g., Cooke et al., 2020). ω_z can be derived from local displacement gradients according to equation 1:

$$\omega_z = \frac{\partial v}{\partial x} - \frac{\partial u}{\partial y} \tag{1}$$

With u and v being the horizontal displacement components in the x, and y direction, respectively. Due to convention, positive and negative ω_z values refer to sinistral and dextral shear sense, respectively. Postprocessing includes an outlier filter to fill gaps of pixels within a 3 by 3 neighbourhood (Westerweel

https://doi.org/10.5194/egusphere-2024-852
Preprint. Discussion started: 28 March 2024

and Scarano, 2005). Discarded vectors in the displacement fields are replaced by an iterative interpolation requiring at least two neighboring vectors. When summing up incremental displacement fields, flow advection due to applied velocities are considered using the Lagrangian sum of displacements (Boutelier et al., 2019). We determined incremental and cumulative vorticity for each time step, i.e., at every 30 seconds.

2.2. Analogue materials

We use two different types of granular materials in our analogue models to assess the role of vertical rheological contrasts in the upper crust: quartz sand and microbeads grains. The quartz sand (distributor Carlo Bernasconi AG; www.carloag.ch) has a grain size between 60 and 250 µm, whereas the grain size of the microbeads (distributor: Worf Glasskugeln, Germany) lies between 150 and 210 µm. Quartz sand and microbeads deform according to the Coulomb failure criterion and have internal peak friction angles of 36° and 22° and cohesion values of 48 ± 26 Pa and 25 ± 4 Pa, respectively (Panien et al., 2016; Zwaan et al., 2018c; Schmid, 2023). The considerable difference in the internal peak friction angle between the two materials makes them suitable for simulating contrasting upper crustal, brittle rheology. Considering their differences between their internal friction angle, we are going to assume through the entire manuscript that the microbeads and quartz sand are weak and strong materials respectively.

The granular materials are sieved on top of a viscous layer representing the lower ductile crust (Fig. 1b). This viscous layer, placed directly on top of the plexiglass bars, consists of a mixture of SGM-36 polydimethylsiloxane (PDMS) and corundum sand (weight ratio of 0.965: 1.000), which has a density of 1600 kgm^{-3}. The mixture has a quasi-linear viscosity of 1.5 ×10^{5} Pa s and a stress exponent of 1.05 (Zwaan et al., 2018c). The properties of all materials are summarized in Table 1.

Granular materials	Quartz sand	Microbeads
Density ρ (kg/m3)	1560	2300
Grain size (µm)	60-250	150-210
Friction coefficient µ	0,72	0,41
Angle of internal Friction °	36°	22,3°
Dynamic stable friction	31,4°	20,6°
Reactivation friction angle (ϕp)	33,4°	21,9°
Cohesion (Pa)	48+-26	25+-4
Viscous mixture	**PDMS**	
Density (Kg/m^3)	1600	
Viscosity η (Pa·s)	150000	

Table 1: Materials properties. For properties of microbeads (Panien et al 2006., Zwaan et al., 2022; Schmid et al., 2022) Viscous mixture: Polydimethylsiloxane (PDMS) mixed with corundum sand; 1:1 weight ratio.

https://doi.org/10.5194/egusphere-2024-852
Preprint. Discussion started: 28 March 2024

2.3. Scaling

The scaling of the models is based on Hubbert (1937) and Ramberg (1981). The brittle materials are scaled using the dynamic similarity equation obtained from the scale's ratios (equation 2). Where ρ^*, g^*, h^* and η^* are the density, gravity, length, and viscosity. The asterisk indicates the ratio of model to nature for that component. The stress ratio is approximately $\sigma^* = 1.13\times10^{-6}$, with 1 cm in the models representing 5 km in nature (Table 2).

$$\sigma^*=\rho^*g^*h^* \qquad (2)$$

Assuming a lower crustal viscosity of $\eta = 10^{22}$ Pa s (Moore and Parsons, 2015; Zhang and Sagiya, 2017) yields a viscosity scaling ratio $\eta^* = 10^{-17}$, which gives $1.13\text{x}10^{11}$ for the strain rate ratio (ε^*) calculated with equation 3, which correlates the stress ratio (σ^*) and the viscosity ratio (η^*).

$$\varepsilon^*=\sigma^*/\eta^* \qquad (3)$$

In order to verify that the dynamic similarities in the models, the Smoluchowski (S_m) and Ramberg (R_m) numbers were determined. The first one (Equation 4) describes the ratio between gravitational stress and cohesive strength (Ramberg, 1981). Where ρ, h, C and μ are the density, thickness, cohesion and friction coefficient, respectively. The second, R_m, describes the ratio between gravitational and viscous stresses (Equation 5; Ramberg, 1981). Model parameters and non-dimensional numbers are given in Table 2.

$$Sm = \rho gh/C+\mu\rho gh \qquad (4)$$

$$Rm = \rho gh^2/\eta v \qquad (5)$$

	General parameters			Brittle upper crust		Ductile lower crust		Smoluchowski (Sm)	Ramberg (Rm)	Reynolds (Re)
	Gravity (m/s2)	Thickness h (m)	Velocity (m s− 1)	Density ρ (kg/m3)	Cohesion (Pa)	Density ρ (kg/m3)	Viscosity η (Pa·s)			
Model	9,81	4,00E-02	2,80E-06	1560	50,00	1600	1,00E+05	1	22	<<1
Nature	9,81	2,00E+04	1,23E-11	2750	5,00E+07	2900	1,00E+22	1	20	<<1
	σ*	ρ*	g*	h*	c*	ε*	η*	v*	t*	
	1,13E-06	0,57	1,00E+00	2,00E-06	1,20E+00	1,13E+11	1,00E-17	2,27E+05	8,81E-12	

Table 2: Scaling parameters and scaling ratios for the reference model Setup with a Brittle Ductile Thickness Ratio T_{BD} = 1

https://doi.org/10.5194/egusphere-2024-852
Preprint. Discussion started: 28 March 2024

3. Results

3.1. Series A. Fault evolution without vertical rheological contrast

The Series A models consist of a homogeneous upper crustal layer composed of a brittle layer of either quartz sand (Fig. 3; Model A1) or microbeads (Fig. 3; Model A2). The incremental strain panels document that strain localizes first in the model with quartz sand, while deformation is still diffuse in the model with microbeads (Fig. 3a and f). With increasing deformation, slightly overlapping right-stepping *en echelon* faults with a sinistral strike-slip displacement form (Fig. 3b and g). In the experiment with quartz sand (Model A1) the first faults to form strike N70°E (Fig. 3b), whereas the initial faults in the experiment with microbeads (Model A2) strike N80˚E (Fig. 3g). Initial deformation in both models is accommodated only by synthetic (sinistral) strike-slip faults (Fig. 3a, b and f, g). As deformation progresses, individual fault segments link up to form through-going major strike-slip faults (Fig 3c and h). At later stages in the model evolution, the model A2 (composed only by microbeads grains) contains more faults than the model A1 (Fig. 3d and i). The model A1 (only quartz sand) is the only one that develops antithetic (dextral) faults. The final cumulative strain panels for both models (Fig. 3e and j) show that most deformation is taken up by a central strike-slip fault that crosses the entire length of the model.

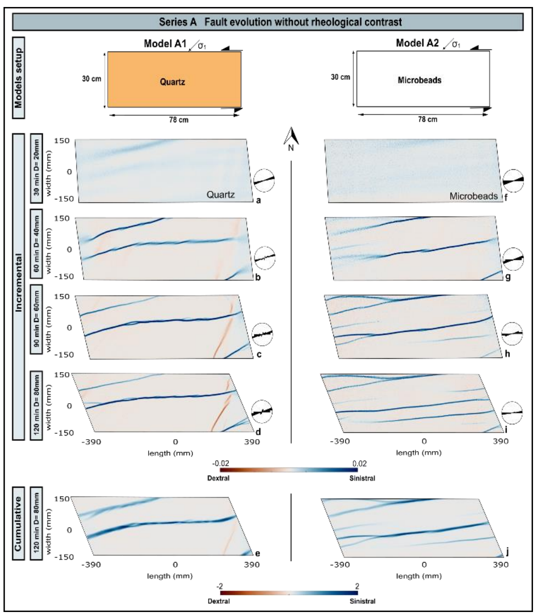

Figure 3: Overview of Series A models: simple shear experiments of models with microbeads (Model A1) and quartz sand (Model A2). Incremental and cumulative positive/negative values indicates dextral and sinistral kinematics, respectively.

https://doi.org/10.5194/egusphere-2024-852
Preprint. Discussion started: 28 March 2024

3.2. Series B. Fault evolution with N-S rheological contrast

The Series B models have rheological contrasts-oriented N-S. Model B1 has a 5-cm wide central contrast of microbeads with quartz sand on either side, whereas in Model B2 it is the other way around (Fig. 4). The contrast divides the model in a western and eastern domain, with the central contrast rotating counterclockwise due to the applied sinistral bulk shear.

In both models, initial simple shear results in reactivation of the N-S rheological boundaries. These are reactivated, showing dextral strike-slip movement (Fig. 4a, f). The antithetical faults are the first ones generated, firstly in model B1. As in the previous series, the models with microbeads grains take longer to localize the deformation. With increasing shearing, deformation tends to be compartmentalized and two domains are distinguished in both models. In Model B1, sinistral, synthetic faults form in the eastern domain whereas both sinistral and dextral faults form in the western domain (Fig, 4c). In contrast, in Model B2, it is the other way around, the eastern domain contains both sinistral and dextral faults, whereas the western domain shows sinistral faulting (Fig. 4h). In both models, the antithetic, dextral strike-slip faults in the western (Model B1) and eastern domains (Model B2) are striking at different angles than those along the vertical contacts of the central contrast. Whereas the reactivated dextral faults along the vertical N-S contacts initially strike N-S, the newly formed dextral faults in the adjacent domains strike N20°E. Model B1 and N7-10°E in Model B2. Because of the bulk sinistral simple shear, the central band and the dextral faults at both contacts rotate counterclockwise, and as they propagate, they acquire a slight S-shape in surface view (Fig. 4b, g). Sinistral faults developed in Model B1 propagate along strike crosscutting the central weak band composed of microbeads, striking W-E in the central domain which differs from the initial strike (Fig. 4c, d). At the same time, the dextral reactivation along the vertical contacts diminishes. However, in Model B2 no sinistral faults cut the central strong contrast composed of quartz sand. This model shows is a greater number of sinistral faults than Model B1. These faults are located in the microbeads, maintain the same spacing between them (fig. 4h and i).

The cumulative strain panels show for both models that most of the deformation is accommodated by sinistral faults, with dextral fault activity restricted to the western domain in Model B1 and to the eastern domain in Model B2 (Fig. 4e, j).

https://doi.org/10.5194/egusphere-2024-852
Preprint. Discussion started: 28 March 2024

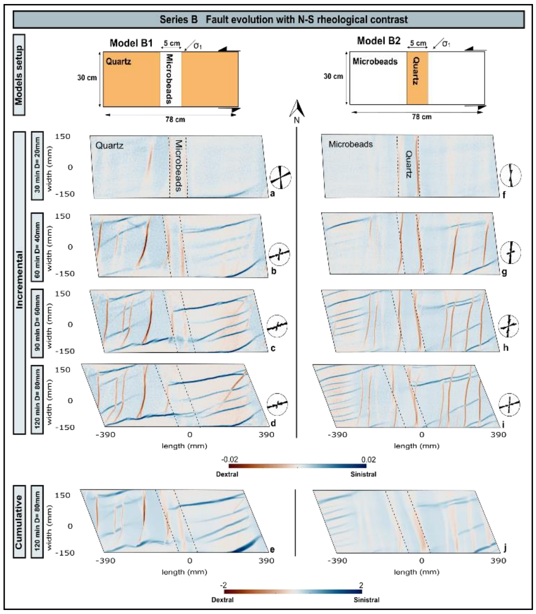

Figure 4: Overview of Series B models: simple shear experiments with a vertical N-S oriented rheological contrast consisting of a 5 cm wide band of microbeads (Model B1) or quartz sand (Model B2) in the central part of the model. Incremental and cumulative positive/negative values indicates dextral and sinistral kinematics, respectively.

3.3. Series C. Fault evolution with N20°W rheological contrast

In the series C models the vertical rheological contrasts oriented N20˚W, with a 5 cm-wide central band of microbeads and quartz sand on either side, in Model C1 and vice versa in Model C2 (Fig. 5). In contrast to the Model B series, no reactivation of the rheological contacts occurs in these series. After 1 hour, two synthetic sinistral faults are generated in Model C1 (Fig. 5b) at the corners of the model, while Model C2 only develop one sinistral fault in the eastern corner (Fig. 5g). The strike of the synthetic faults varies between the two models, N76˚E in Model C1 (Fig. 5c) and N80˚E in Model C2. The same occurs with the antithetic faults developed at the end of the models. The antithetic faults strike N27˚E in Model C1 (Fig. 5c, d) and N9˚E in Model C2.

https://doi.org/10.5194/egusphere-2024-852
Preprint. Discussion started: 28 March 2024

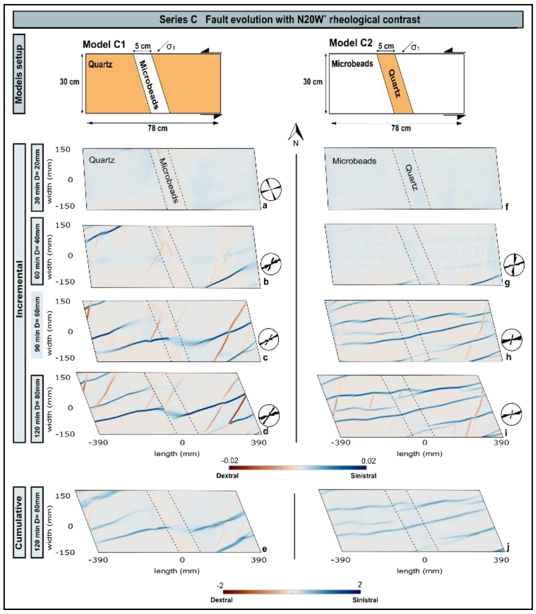

Figure 5: Overview of Series C models: simple shear experiments with a vertical N20˚ W rheological contrast consisting of a 5 cm wide band of microbeads (Model C1) or quartz sand (Model C2) in the central part of the model. Incremental and cumulative positive/negative values indicate dextral and sinistral kinematics, respectively.

In these models' series, the introduction of the central contrast does not affect the behavior of both models and there are no domains. There are more sinistral faults in model C2 than in model C1 (Fig. 5c and h), and both cut the central band. In Model C1, when these faults reach the contact with the microbeads, they change their strike turning clockwise, resulting in an overall E-W releasing band (Fig. 5c, d). At the same time, deformation in the central band is less localized. Unlike Model C1, the synthetic sinistral faults in Model C2 change its strike counterclockwise when they cut the central contrast (Fig. 5i).

The cumulative strain panels clearly show that most deformation in both models is taken up by synthetic, sinistral faults. Model C1 shows little deformation in the central domain with synthetic faults abutting at the rheological contrast on either side, with diffuse deformation within the central band. In contrast, Model C2 shows synthetic faults throughout the model cutting across the central domain of quartz sand with deformation being less diffuse in the central domain.

3.4. Series D. Fault evolution with N20˚E rheological contrast

https://doi.org/10.5194/egusphere-2024-852
Preprint. Discussion started: 28 March 2024

The vertical rheological contacts in the Series D models oriented N20°E, with a 5-cm wide central contrast composed by microbeads surrounded by quartz sand in Model D1 and vice versa in Model D2 (Fig. 6). As in the models' series B, the rheological boundaries are reactivated with dextral strike-slip movement (Fig. 6a and f) and three fault domains are generated. With increasing shearing, model D1 develops 5 sinistral faults (Fig. 6 b). In contrast, model D2 only develop one clear sinistral fault and the antithetic faults begin to show slightly in the model (Fig. 6g). As in the previous models, the strike of these synthetic faults varies. The synthetic faults in the quartz sand strike N77˚E, whereas in the microbeads is N80˚E. In Model D2, the antithetic faults strike N7˚E become more prominent, particularly in the western domain. They accommodate more displacement and rotate at the same time counterclockwise with almost N-S orientation (Fig 6h, i). Unlike Model D2, Model D1 barely registers antithetic faults, and their strike is N17˚E. Although the model with predominantly microbeads(D2) takes longer to localized the deformation, it registers a greater number of faults at the end than the model with predominantly quartz sand (D1).

In both models, localized deformation is not transferred through the central band and the sinistral faults do not connect (Fig. 6c and h). With increasing shear, despite the predominance of dextral faults in model D2, the cumulative strain panels (Fig. 6e, j) clearly show the dominance of sinistral strike-slip faulting in the western and eastern domains for both models.

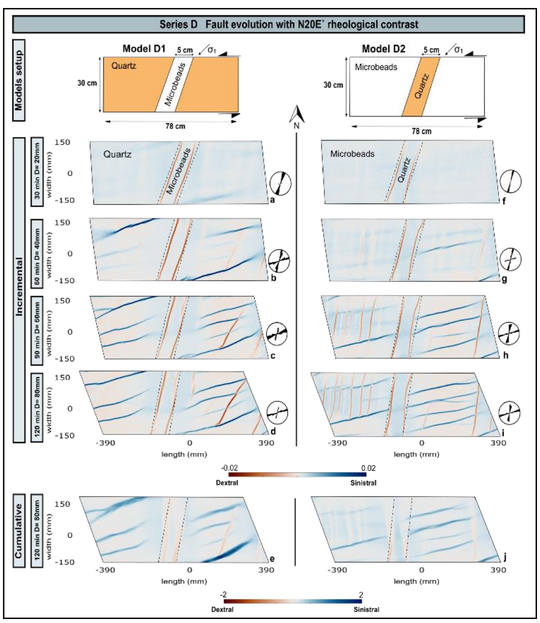

https://doi.org/10.5194/egusphere-2024-852
Preprint. Discussion started: 28 March 2024

Figure 6: Overview of Series D models: simple shear experiments with a vertical N20° lithology contrast band 5 cm, composed of microbeads grains (Model D1) and quartz sand (Model D2). Incremental and cumulative positive/negative values indicate dextral and sinistral kinematics. respectively.

4. Discussion

We used granular materials with contrasting rheologies to test the influence of vertical contrasts on the development and evolution of strike-slip fault zones. It must be noted that the vertical lithological boundaries are reactivated during model construction when the thin cardboard sheets, used to separate the two granular materials, are removed.

We first discuss the results of our models without any vertical rheological contrast (4.1). Then, we are going to discuss the obtained results from the addition a vertical contrast in the model (4.2) Finally, we compare our results with a natural example (4.3).

4.1. Models without vertical rheological contrast

In our models without a vertical rheological contrast (Models A1 and A2), the deformation is accommodated by synthetic, sinistral strike-slip faults (Fig. 7a and i). The deformation takes more time to be localized in models containing the weak material (model composed only by microbeads grains; Model A2; Fig. 7i and m) than in models composed by the strong material (model composed only by quartz sand; Model A1; Fig. 7a and e). However, the experiment composed by this weaker and rounded material shows the highest number of faults at the end of the experiment (Model A2) (Fig. 7i). This phenomenon could be due to the size and shape of the materials. The more equal are the grain size and shape, like microbeads grains, the less deformation concentrate (Antonellini et al., 1994., Mair et al., 2002). This deformation pattern was also observed by Aydin and Berryman, 2010; Li et al., 2021; Cheng et al., 2022 and Venancio and Alves Da Silva, 2023.

The strike of the faults in the models with the strong material is N72°E (Fig. 7e). On the contrary, the initial strike of the faults in models with weaker material is N81°E (Fig. 7m). As the granular materials have a coefficient of internal friction of 36° for quartz sand and 22° for microbeads (Anderson, 1951; Panien et al., 2006; Dooley & Schreurs, 2012) they have a different rupture criteria (Mohr-Coulomb).

4.2. Models with a vertical rheological contrast

When a horizontal rheological contrast is imposed, a series of changes in the stress field are induced, resulting in different kinematics and fault propagation patterns (Segall and Pollard, 1983; Peacock, 1991; Peacock and Sanderson, 1992; Livio et a., 2020). In addition, the heterogeneity of the models is determinant for the structure and chronology of the faults (Viola et al., 2004; Schellart and Strak, 2016; Lefevre et al., 2020; Venancio and Alves Da Silva, 2023).

As in the article from Gomes et al (2019), in our models, the addition of a *vertical* rheological contrast results also in different fault patterns comparing with models without a vertical contrast. Moreover, the fault patterns became more complex considering the orientation of the vertical contact. The introduction of a vertical contrast oriented N-S and N20˚E, influences on: (1) the number of faults is greater if the contrasts are N-S oriented (Fig. 7c and k); (2) greater number of antithetic faults. (Fig. 7o and p). These setups create two domains with rectangular shapes (shorter on the X axis and longer on the Y axis), inducing the model to be compartmentalized. This geometry will change the final fault pattern and promotes the development of antithetic, dextral faults (Garfunkel and Ron, 1985; Capais et al., 1991; Dooley and Schreurs, 2012).

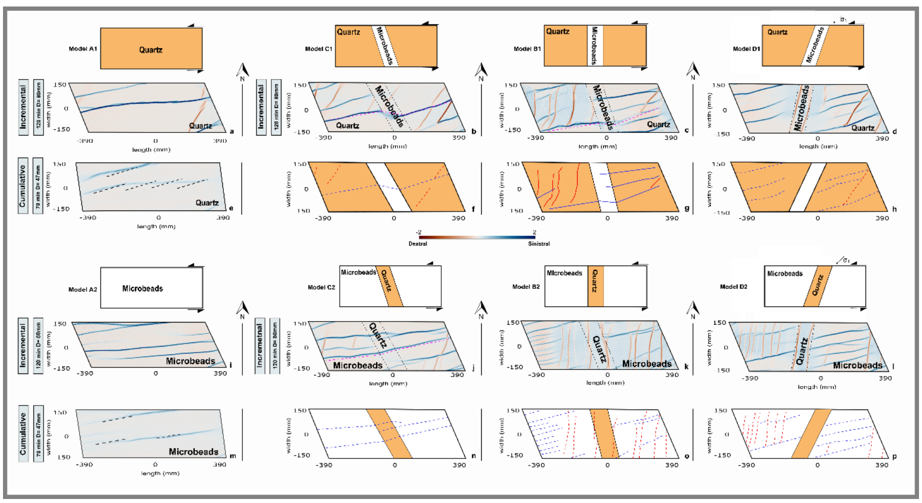

Figure 7: Overview of the main stages of the experiment with schematic drawings depicting the final result.

The initial strike of the antithetic, dextral faults is N10˚E in zones composed by the weak material and N7˚E in the strong materials. However, as the models progress the final fault strike for both types of models

https://doi.org/10.5194/egusphere-2024-852
Preprint. Discussion started: 28 March 2024

became more N-S and showing a S-shape for the models with the weak material in the center (Fig. 7o and p). This phenomenon could be related to block rotation (Garfunkel and Ron, 1985; Deng et al., 1986), which is a process that occurs in nature (Ron et al., 1984, 1986; Nicholson et al., 1986; Sylvester, 1988; Sorlien et al., 1999; Dooley and Schreurs, 2012; Kavyani-Sadr et al., 2022). The initial strike of the synthetic, sinistral faults remains the same during the whole experiment, being N70°E for models predominating the strong material and N80°E for models with the weak one (Fig. 7b and j).

If the central contrast is oriented N20°E, the faults do not cut the contacts (even when the material is the weaker one; Fig. 7h and p). When the contrast is oriented N-S and is composed of the strong material, the faults do not cut the rheological contrast (Fig. 7k and o). However, if the weaker material constitutes the rheological contrast, the sinistral faults crosscut the contact changing their strike from N70ºE to E-W (Fig. 7c and g). The only series models that show faults cutting the contrast, despite the properties of the material, are the models with the oriented contrasts N20˚W (models C1 and C2; Fig. 7b, f, j and n). If the contrast is constituted of a weaker material, the initial fault strike turns clockwise to a more like E-W as in model B1 (Fig. 7f). On the contrary, the faults that crosscut the strong material turns counterclockwise striking approximately N45˚E (Fig. 7n). This change in the strike of the faults could be related to the internal friction angle of the unit cut (Du and Ayin, 1995; de Doney et al., 2011).

4.3. Natural example

The NW Iberian Peninsula is located in the Iberian Massif (Fig. 8a), a Variscan basement (Paleozoic in age) deformed during two orogeny processes: the Variscan and the Alpine Orogenies (Arthaud and Matte, 1975; Vegas et al., 2004; Martín-González and Heredia, 2011; Martínez Catalán, 2012; Gutiérrez-Alonso et al., 2015; Díez Fernández and Pereira, 2016). The area contains two major intraplate fault systems: the Penacova-Régua-Verin (PRV) and the Manteigas-Vilariça-Bragança (MVB) (Fig. 8b). These NNE-SSW left-lateral strike-slip faults are longer than 200 km and crosscut three main lithologies domains, from stronger to weaker: (1) Bragança-Morais Complex, (2) Granites and (3) Schist-Greywacke Complex.

https://doi.org/10.5194/egusphere-2024-852
Preprint. Discussion started: 28 March 2024

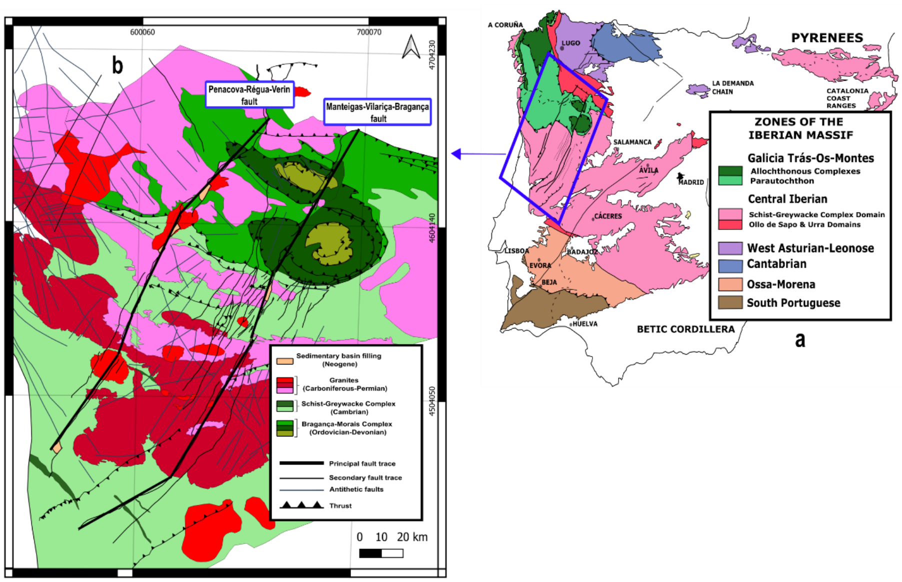

Figure 8: a) Geological map of the Iberian Massif and the location of the natural example (modified from Martínez-Catalán, 2012 and Martín-González & Hereida, 2011). b) Schematic geological map of the NW of the Iberian Peninsula showing the main fault orientations at the different units. The antithetic faults are also represented following a NW-SE orientation.

The PRV and MVB fault systems show different deformation patterns depending on the lithologies crossed like more parallel faults traces in the weak resistant units, or changes in the strike of the principal trace (Fig. 8). The pattern observed in the faults are comparable with our results in the analogue modelling experiments (e.g., models B1 and C1). The number of secondary fault traces are not the same. There is a greater number of secondary fault traces in the central section of the MVB fault, constituted essentially by slates that could be represented by the microbeads from models B2 and D2 (Panien et al., 2006). The region shows sinistral and antithetical faults mainly located in metamorphic units and granites respectively. The sinistral Penacova-Régua-Verin and Manteigas-Vilariça-Bragança faults are the main drivers for the recorded displacement, and the principal trace of both faults changes the strike after crosscut the lithologies with different rheology as in the models B1 and C1.

https://doi.org/10.5194/egusphere-2024-852
Preprint. Discussion started: 28 March 2024

5. Conclusions

This study evaluates the influence of vertical rheological contrasts using analogue models inspired by the deformation patterns of the strike-slip fault. Our study shows that the fault types and their evolution depend on the characteristic of the lithology and its contact orientation.

If the lithology is weak, in terms of low value of internal friction angle, the initial deformation is rather diffuse and thus difficult to see. In weak materials, localized deformation does not show up as fast as in stronger material; however, at the end they register a greater number of faults than the strong material.

The faults do not cut the rheological contrast if this is oriented oblique with respect to the shear direction, even though it is composed of weak material. The faults cut the contrast if this is oriented towards the shear direction, or when the contacts of the contrast are perpendicular to the shear direction and is composed by the weak material.

The initial fault's strike changes when they crosscut cut a new lithology. If the material is weak, the fault changes its initial strike clockwise. If the contrast is composed of the strong material, the initial fault strike changes anticlockwise.

Our results are comparable with the fault systems observed in the NW of the Iberian Peninsula. The faults main traces change their initial strike when they crosscut different geological units. The are a greater number of sinistral faults located in the weak units (slates).

6. Competing interests

The contact author has declared that none of the authors has any competing interests.

7. Acknowledgments

The following work has been partially funded by a predoctoral contract (PREDOC20-073), by the Universidad Rey Juan Carlos and project PID2022-139527OB-I00 funded by MCIN/AEI/10.13039/501100011033/ and FEDER.

https://doi.org/10.5194/egusphere-2024-852
Preprint. Discussion started: 28 March 2024

8. References

Aki, K.: Geometric features of a fault zone related to the nucleation and termination of an earthquake rupture, in: Proceedings of Conference XLV Fault Segmentation and Controls of Rupture Initiation and Termination. US Geological Survey Open File Report 89-315, pp. 1–9, 1989

Arthaud, F., Matte, Ph.: Les decrochements tardi-hercyniens du sud-ouest de l'europe. Geometrie et essai de reconstitution des conditions de la deformation. Tectonophysics 25, 139–171. https://doi.org/10.1016/0040-1951(75)90014-1, 1975.

Anderson, E. M: The Dynamics of faulting and Dyke Formation with Applications to Britain (2nd edition), Oliver and Boyd, Edinburgh, Scotland, 1951.

Antonellini, M.A., Aydin, A., Pollard, D.D.: Microstructure of deformation bands in porous sandstones at Arches National Park, Utah. Journal of Structural Geology 16, 941e959, 1994.

Aydin, A., Nur, A.: Evolution of pull-apart basins and their scale independence. Tectonics 1, 91–105, 1982.

Aydin, A.: Fractures, faults, and hydrocarbon entrapment, migration and flow. Marine and Petroleum Geology 17, 797–814, 2000.

Aydin, A., & Berryman, J. G: Analysis of the growth of strike-slip faults using effective medium theory. *Journal of Structural Geology*, *32*(11), 1629–1642. https://doi.org/10.1016/j.jsg.2009.11.007, 2010.

Barka, A., Kadinsky-Cade, K.: Strike-slip fault geometry in Turkey and its influence on earthquake activity. Tectonics 7, 663–684, 1988.

Boutelier, D., Schrank, C., Regenauer-Lieb, K.: 2-D finite displacements and strain from particle imaging velocimetry (PIV) analysis of tectonic analogue models with TecPIV. Solid Earth 10, 1123-1139, 2019.

Burgmann, R., Pollard, D.D.: Strain accommodation about strike-slip fault discontinuities in granitic rock under brittle-to-ductile conditions. Journal of Structural Geology 16, 1655–1674, 1994.

Cazarin, C.L., van der Velde, R., Santos, R.V., Reijmer, J.J.G., Bezerra, F.H.R., Bertotti, G., La Bruna, V., Silva, D.C.C., de Castro, D.L., Srivastava, N.K., Barbosa, P. F.: Hydrothermal activity along a strike-slip fault zone and host units in the S˜ ao Francisco Craton, Brazil – implications for fluid flow in sedimentary basins. Precambrian Res. 365 https://doi.org/10.1016/j.precamres.2021.106365, 2021.

Cheng, X., Ding, W., Pan, L., Zou, Y., Li, Y., Yin, Y., & Ding, S.: Geometry and kinematics characteristics of strike-slip fault zone in complex structure area: A case study from the south no. 15 strike-slip fault zone in the Eastern Sichuan Basin, China. Frontiers in earth science, 10. https://doi.org/10.3389/feart.2022.922664, 2022.

Cooke, M. L., Toeneboehn, K., and Hatch, J. L.: Onset of slip partitioning under oblique convergence within scaled physical experiments, Geosphere, 16, 875-889. https ://doi.org/10.1130/GES02179.1, 2020.

de Joussineau, G., & Aydin, A.: Segmentation along strike-slip faults revisited. *Pure and Applied Geophysics*, *166*(10–11), 1575–1594. https://doi.org/10.1007/s00024-009-0511-4, 2009.

Deng, Q., Wu, D., Zhang, P., & Chen, S.: Structure and deformational character of strike-slip fault zones. Pure and Applied Geophysics, 124(1–2), 203–223. https://doi.org/10.1007/bf00875726, 1986.

Díez Fernández, R., Pereira, M.F.: Extensional orogenic collapse captured by strike-slip tectonics: Constraints from structural geology and UPb geochronology of the Pinhel shear zone (Variscan orogen, Iberian Massif). Tectonophysics 691, 290–310. https ://doi.org/10.1016/j.tecto.2016.10.023, 2016.

Dooley, T. P., & Schreurs, G. : Analogue modelling of intraplate strike-slip tectonics: A review and new experimental results. *Tectonophysics*, *574–575*, 1–71. https://doi.org/10.1016/j.tecto.2012.05.030, 2012

Du, Y., & Aydin, A.: Shear fracture patterns and connectivity at geometric complexities along strike-slip faults. *Journal of Geophysical Research*, *100*(B9), 18093–18102. https://doi.org/10.1029/95jb01574, 1995.

https://doi.org/10.5194/egusphere-2024-852
Preprint. Discussion started: 28 March 2024

Gamond, J.F.: Displacement features associated with fault zones: a comparison between observed examples and experimental models. Journal of Structural Geology 5, 33–45, 1983.

Garfunkel, Z., & Ron, H.: Block rotation and deformation by strike-slip faults: 2. The properties of a type of macroscopic discontinuous deformation. Journal of Geophysical Research, 90(B10), 8589–8602. https://doi.org/10.1029/jb090ib10p08589, 1985.

Gomes, A. S., Rosas, F. M., Duarte, J. C., Schellart, W. P., Almeida, J., Tomás, R., & Strak, V.: Analogue modelling of brittle shear zone propagation across upper crustal morpho-rheological heterogeneities. *Journal of Structural Geology*, *126*, 175–197. https://doi.org/10.1016/j.jsg.2019.06.004, 2019.

Gutiérrez-Alonso, G., Collins, A. S., Fernández-Suárez, J., Pastor-Galán, D., González-Clavijo, E., Jourdan, F., Weil, A. B., & Johnston, S. T.: Dating of lithospheric buckling: 40Ar/39Ar ages of syn-orocline strike–slip shear zones in northwestern Iberia. *Tectonophysics*, *643*, 44–54. https://doi.org/10.1016/j.tecto.2014.12.009, 2015.

Harris, R.A., Day, S.M.: Dynamic 3D simulation of earthquakes on en echelon faults. Geophysical Research Letters 26, 2089–2092, 1999.

Hubbert, M. K.: Theory of scale models as applied to the study of geologic structures. The Geological Society of America Bulletin, 48(10), 1459–1520. https://doi.org/10.1130/GSAB-48-1459, 1937.

Kavyani-Sadr, K., Rahimi, B., Khatib, M.M., Kim, Y.-S.: Assessment of open spaces related to Riedel-shears dip effect in brittle shear zones. J. Struct. Geol. 154, 104486 https://doi.org/10.1016/j.jsg.2021.104486, 2022.

Kim, Y., Peacock, D.C.P., Sanderson, D.J.: Fault damage zones. Journal of Structural Geology 26, 503–517, 2004.

Kirkland, C. L., Alsop, G. I., & Prave, A. R.: The brittle evolution of a major strike-slip fault associated with granite emplacement: a case study of the Leannan Fault, NW Ireland. Journal of the Geological Society, 165(1), 341–352. https://doi.org/10.1144/0016-76492007-064, 2008.

Lefevre, M., Souloumiac, P., Cubas, N., & Klinger, Y. : Experimental evidence for crustal control over seismic fault segmentation. Geology, 48(8), 844–848. https://doi.org/10.1130/g47115.1, 2020.

Livio, F. A., Ferrario, M. F., Frigerio, C., Zerboni, A., & Michetti, A. M.: Variable fault tip propagation rates affected by near-surface lithology and implications for fault displacement hazard assessment. Journal of Structural Geology, 130(103914), 103914. https://doi.org/10.1016/j.jsg.2019.103914, 2020.

Mair, K., Frye, K.M., Marone, C.: Influence of grain characteristics on the friction of granular shear zones. Journal of Geophysical Research 107 (B10), 4/1-4/9, 2002.

Martel, S.J., Peterson Jr., J.E.: Interdisciplinary characterization of fracture systems at the US/BK site, Grimsel Laboratory, Switzerland. International Journal of Rock Mechanics and Mining Science and Geomechanical Abstracts 28, 259–323, 1991.

Martínez Catalán, J.R. : The Central Iberian arc, an orocline centered in the Iberian Massif and some implications for the Variscan belt. Int. J. Earth Sci. 101, 1299–1314. https://doi.org/10.1007/s00531-011-0715-6, 2012.

Martín-González, F., Heredia, N.: Geometry, structures and evolution of the western termination of the Alpine-Pyrenean Orogen reliefs (NW Iberian Peninsula). J. Iber. Geol. 37, 103–120. https://doi.org/10.5209/rev_JIGE.2011.v37.n2.1, 2011.

Moore, J. D. P., & Parsons, B.: Scaling of viscous shear zones with depth-dependent viscosity and power-law stress–strain-rate dependence. *Geophysical Journal International*, *202*(1), 242–260. https://doi.org/10.1093/gji/ggv143, 2015.

Myers, R., Aydin, A.: The evolution of faults formed by shearing across joint zones in sandstone. Journal of Structural Geology 26, 947–966, 2004.

Nicholson, C., Seeber, L., Williams, P. and Sykes, L.R.: Seismic evidence for conjugate slip and block rotation within the San Andreas fault system, Southern California. Tectonics, 5: 629-648, 1986

Odling, N.E., Harris, S.D., Knipe, R.J.: Permeability scaling properties of fault damage zones in siliclastic rocks. Journal of Structural Geology 26, 1727–1747, 2004.

Panien, M., Schreurs, G., & Pfiffner, A.: Mechanical behaviour of granular materials used in analogue modelling: insights from grain characterisation, ring-shear tests and analogue experiments. *Journal of Structural Geology*, *28*(9), 1710–1724. https://doi.org/10.1016/j.jsg.2006.05.004, 2006.

Peacock, D.C.P., Sanderson, D.J.: Displacement, segment linkage and relay ramps in normal fault zones. Journal of Structural Geology 13, 721–733, 1991.

https://doi.org/10.5194/egusphere-2024-852
Preprint. Discussion started: 28 March 2024

Peacock, D. C. P., & Sanderson, D. J.: Effects of layering and anisotropy on fault geometry. *Journal of the Geological Society*, *149*(5), 793–802. https://doi.org/10.1144/gsjgs.149.5.0793, 1992.

Petersen, M. D., Dawson, T. E., Chen, R., Cao, T., Wills, C. J., Schwartz, D. P., & Frankel, A. D.: Fault displacement hazard for strike-slip faults. *Bulletin of the Seismological Society of America*, *101*(2), 805–825. https://doi.org/10.1785/0120100035, 2011.

Preuss, S., Herrendörfer, R., Gerya, T., Ampuero, J.-P., & Dinther, Y.: Seismic and aseismic fault growth lead to different fault orientations. Journal of Geophysical Research. Solid Earth, 124(8), 8867–8889. https://doi.org/10.1029/2019jb017324, 2019.

Ramberg, H.: Gravity, deformation and the Earth's crust: In theory, experiments and geological application (p. 452). Academic Press, 1981.

Richard, P.: Experiments on faulting in a two-layered cover sequence overlying a reactivated basement fault with oblique-slip. J. Struct. Geol. 13, 459–469, 1991.

Richard, P., Naylor, M.A., Koopman, A.: Experimental models of strike-slip tectonics. Petroleum Geoscience 1, 71–80, 1995.

Rispoli, R.: Stress fields about strike-slip faults inferred from stylolites and tension gashes. Tectonophysics 75, 729–736, 1981.

Ron, H., Freund, R., Garfunkel, Z. and Nur, A.: Block rotation by strike slip faulting: structural and paleomagnetic evidence. J. Geophys. Res., 89: 6256-6270, 1984.

Schellart, W.P., Strak, V.: A review of analogue modelling of geodynamic processes: Approaches, scaling, materials and quantification, with an application to subduction experiments. J. Geodyn. 100, 7–32. https://doi.org/10.1016/j. jog.2016.03.009, 2016.

Schmid, T. C., Schreurs, G., & Adam, J.: Rotational extension promotes coeval upper crustal brittle faulting and deep-seated rift-axis parallel flow: Dynamic coupling processes inferred from analog model experiments. *Journal of Geophysical Research. Solid Earth*, *127*(8). https://doi.org/10.1029/2022jb024434, 2022.

Schmid, T. C., Brune, S., Glerum, A., & Schreurs, G.: *Tectonic interactions during rift linkage: Insights from analog and numerical experiments*. https://doi.org/10.5194/egusphere-2022-1203, 2023

Scholz, C. H.: *The Mechanics of Earthquakes and Faulting*. Cambridge University Press, 2002.

Segall, P., & Pollard, D. D.: Nucleation and growth of strike slip faults in granite. *Journal of Geophysical Research*, *88*(B1), 555. https://doi.org/10.1029/jb088ib01p00555, 1983.

Shaw, B.E., Dieterich, J.H.: Probabilities for jumping fault segment stepovers. Geophysical Research Letters 34, L01307. doi:10.1029/2006GL027980, 2007.

Sibson, R.H.: Stopping of earthquake ruptures at dilational fault jogs. Nature 316, 248–251, 1985.

Stirling, M.W., Wesnousky, S.G., Shimazaki, K.: Fault trace complexity, cumulative slip, and the shape of the magnitude-frequency distribution for strike-slip faults: a global survey. Geophysical Journal International 124, 833–868, 1996.

Sylvester, A.G.: Strike-slip faults. Geol. Soc. Am. Bull. 100, 1666–1703. https:// doi.org/10.1130/0016-7606(1988)1002.3.CO;2, 1988.

Venâncio, M. B., & da Silva, F. C. A.: Structures evolution along strike-slip fault zones: The role of rheology revealed by PIV analysis of analog modeling. Tectonophysics, 229764, 229764. https://doi.org/10.1016/j.tecto.2023.229764, 2023.

Viola, G., Odonne, F., Mancktelow, N.S.: Analogue modelling of reverse fault reactivation in strike–slip and transpressive regimes: application to the Giudicarie fault system, Italian Eastern Alps. J. Struct. Geol. 36, 401–418. https://doi.org/ 10.1016/j.jsg.2003.08.014, 2004.

Wesnousky, S.G.: Seismological and structural evolution of strike-slip faults. Nature 335, 340–342, 1988.

Wesnousky, S.G.: Predicting the endpoints of earthquake ruptures. Nature 444, 358–360, 2006.

Westerweel, J., Scarano, F.: Universal outlier detection for PIV data. Experiments in fluids 39, 1096-1100, 2005.

Zwaan, F., Schreurs, G., Ritter, M., Santimano, T., & Rosenau, M.: Rheology of PDMS-corundum sand mixtures from the Tectonic Modelling Lab of the University of Bern (CH). V. 1. GFZ data Services. https://doi. org/10.5880/fdgeo.2018.023, 2018c

https://doi.org/10.5194/egusphere-2024-852
Preprint. Discussion started: 28 March 2024

Zwaan, F., Schreurs, G., Madritsch, H., & Herwegh, M.: Influence of rheologically weak layers on fault architecture: insights from analogue models in the context of the Northern Alpine Foreland Basin. Swiss Journal of Geosciences, 115(1). https://doi.org/10.1186/s00015-022-00427-8, 2022.